AIAA JOURNAL
Vol. 34, No. 4, April 1996

Three-Dimensional Analytical Solutions for Coupled Thermoelectroelastic Response of Multilayered Cylindrical Shells

Kangming Xu* and Ahmed K. Noor†
University of Virginia and NASA Langley Research Center, Hampton, Virginia 23681

Analytical three-dimensional solutions are presented for the coupled thermoelectroelastic response of multilayered hybrid composite cylindrical shells. The shells consist of a combination of fiber-reinforced cross-ply and thermoelectroelastic layers. Both the thermoelectroelastic static response and its sensitivity coefficients are evaluated. The sensitivity coefficients measure the sensitivity of the response to variations in the different mechanical, thermal, and piezoelectric material properties of the shells. A linear constitutive model is used, and the material properties are assumed to be independent of the temperature and the electric field. A mixed formulation is used with the fundamental unknowns consisting of the three transverse stress components; the three displacement components; the transverse component of the electric displacement field; the electric potential; the transverse heat-flux component; and the temperature change. Each of the fundamental unknowns is expressed in terms of a double Fourier series in the surface coordinates. A state-space approach is used to generate the static response and to evaluate the sensitivity coefficients. The response and sensitivity coefficients of the shell are obtained by using a modified Frobenius method and a sublayer method. Numerical results are presented showing the effects of variation in the geometric parameters of the shells on the different response quantities and their sensitivity coefficients.

I. Introduction

HYBRID composite shells consisting of fiber-reinforced and thermoelectroelastic layers are important components of smart or intelligent structures.[1-3] Analytic three-dimensional solutions for these shells are not only valuable in their own right, but they are also useful for assessing the range of validity of approximate computational models. Analytical three-dimensional solutions of elastic multilayered shells have been presented in previous literature.[4-10] In the cited references, only elastic response quantities are calculated. To the authors' knowledge, no publications exist in which analytical three-dimensional solutions of the fully coupled thermoelectroelastic response of multilayered shells of finite length are presented. Because of the increasing use of hybrid composites in structures,[11-14] it is desirable to develop a capability for the accurate determination of 1) the steady-state response of multilayered hybrid shells, and 2) the sensitivity of the response to variations in the material and lamination parameters. The present study attempts to fill this void.

Specifically, this paper presents analytical three-dimensional solutions for the thermoelectroelastic response of hybrid laminated cylindrical shells. Sensitivity coefficients also are evaluated and used to study the sensitivity of the response to variations in the different material properties of the shells. Two approaches for generating the response and evaluating the sensitivity coefficients are used. The first one is a modified Frobenius method,[10] and the second is a sublayer method.[6,15] Both methods are efficient procedures for obtaining analytical solutions for the shell response and sensitivity coefficients. The shells consist of a number of perfectly bonded thermoelectroelastic and fiber-reinforced layers. The solutions are doubly periodic in the shell surface coordinates. Numerical results are presented showing the effects of variation in the geometric parameters of the shell on the different response characteristics and their sensitivity coefficients. The solutions presented provide physical insight into the interaction between the mechanical, thermal, and electric fields. They also help in the development and assessment of two-dimensional models of multilayered hybrid composite shells.

Received July 27, 1995; revision received Nov. 3, 1995; accepted for publication Nov. 14, 1995.

*Research Associate, Center for Computational Structures Technology. Member AIAA.

†Ferman W. Perry Professor of Aerospace Structures and Applied Mechanics and Director, Center for Computational Structures Technology. Fellow AIAA.

II. Mathematical Formulation

Figure 1 shows the geometric characteristics of the hybrid multilayered cylindrical shell segment considered herein, henceforth referred to as the shell, as follows: L, R, and h are the length, the radius of the middle surface, and the total thickness of the shell, respectively. The cylindrical coordinate system $\{x, \theta, r\}$ and the surface coordinate system for each layer $\{x, \theta, z\}$ $[0 \le z \le h^{(\eta)}]$ used in this study also are given in the figure, where $h^{(\eta)}$ is the thickness of a typical (ηth) layer. The shell has a combination of homogeneous cross-ply orthotropic elastic layers and orthorhombic thermoelectroelastic layers with crystal system 2 mm.

The analytical formulation is based on the linear three-dimensional theory of anisotropic thermoelectroelasticity. The fundamental relations of thermoelectroelastic materials in the cylindrical coordinate system[16,17] are summarized in Appendix A.

The temperature variation T, electric potential ϕ, and the traction components $\{q_x, q_\theta, q_z\}$ at the inner and outer surfaces of the shell are functions of x and θ, i.e.,

$$\begin{aligned} &T^0 = T^0(x,\theta), \qquad T^h = T^h(x,\theta) \\ &\phi^0 = \phi^0(x,\theta), \qquad \phi^h = \phi^h(x,\theta) \\ &q_x^0 = q_x^0(x,\theta), \qquad q_\theta^0 = q_\theta^0(x,\theta), \qquad q_z^0 = q_z^0(x,\theta) \\ &q_x^h = q_x^h(x,\theta), \qquad q_\theta^h = q_\theta^h(x,\theta), \qquad q_z^h = q_z^h(x,\theta) \end{aligned} \tag{1}$$

where the superscripts 0 and h refer to the inner and outer surfaces, respectively.

A. Expansions for Displacement, Stress, Temperature, and Electric Fields

For hybrid cylindrical shells consisting of cross-ply and thermoelectroelastic layers, each of the displacement components $\{u, v, w\}$, stress components $\{\sigma_x, \sigma_\theta, \sigma_z, \tau_{\theta z}, \tau_{xz}, \tau_{x\theta}\}$, electric displacement components $\{d_x, d_\theta, d_z\}$, electric potential ϕ, heat flux components $\{p_x, p_\theta, p_z\}$, and temperature T for each layer, is expressed as the sum of products of trigonometric functions in the surface coordinates. The following expansions are used for the different response quantities:

$$\begin{Bmatrix} u \\ v \\ w \end{Bmatrix} = \sum_{m=0}\sum_{n=0} \begin{Bmatrix} U_{mn}(z)\cos a_m x \cos n\theta \\ V_{mn}(z)\sin a_m x \sin n\theta \\ W_{mn}(z)\sin a_m x \cos n\theta \end{Bmatrix} \tag{2}$$

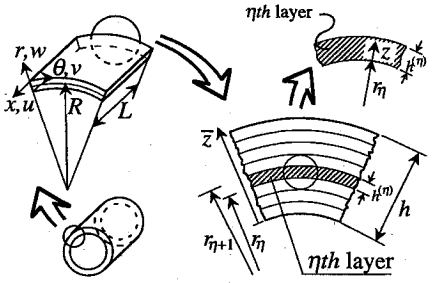

a) Sign convection and shell surface coordinates

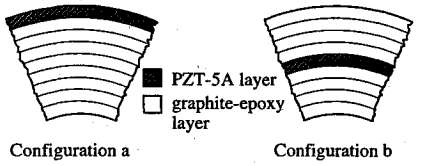

b) Shell configurations used in the numerical study

Fig. 1 Hybrid multilayered composite cylindrical shells.

$$\begin{Bmatrix}\sigma_x\\ \sigma_\theta\\ \sigma_z\end{Bmatrix} = \sum_{m=1}\sum_{n=0}\begin{Bmatrix}S_{xmn}(z)\\ S_{\theta mn}(z)\\ S_{zmn}(z)\end{Bmatrix}\sin a_m x\cos n\theta \tag{3}$$

$$\begin{Bmatrix}\tau_{\theta z}\\ \tau_{xz}\\ \tau_{x\theta}\end{Bmatrix} = \sum_{m=0}\sum_{n=0}\begin{Bmatrix}S_{\theta zmn}(z)\sin a_m x\sin n\theta\\ S_{xzmn}(z)\cos a_m x\cos n\theta\\ S_{x\theta mn}(z)\cos a_m x\sin n\theta\end{Bmatrix} \tag{4}$$

$$\begin{Bmatrix}d_x\\ d_\theta\\ d_z\end{Bmatrix} = \sum_{m=0}\sum_{n=0}\begin{Bmatrix}D_{xmn}(z)\cos a_m x\cos n\theta\\ D_{\theta mn}(z)\sin a_m x\sin n\theta\\ D_{zmn}(z)\sin a_m x\cos n\theta\end{Bmatrix} \tag{5}$$

$$\begin{Bmatrix}p_x\\ p_\theta\\ p_z\end{Bmatrix} = \sum_{m=0}\sum_{n=0}\begin{Bmatrix}P_{xmn}(z)\cos a_m x\cos n\theta\\ P_{\theta mn}(z)\sin a_m x\sin n\theta\\ P_{zmn}(z)\sin a_m x\cos n\theta\end{Bmatrix} \tag{6}$$

$$\phi = \sum_{m=1}\sum_{n=0}\Phi_{mn}(z)\sin a_m x\cos n\theta \tag{7}$$

$$T = \sum_{m=1}\sum_{n=0}T_{mn}(z)\sin a_m x\cos n\theta \tag{8}$$

where $a_m = m\pi/L$. The unknown amplitudes U_{mn}, V_{mn}, W_{mn}, S_{xmn}, $S_{\theta mn}$, S_{zmn}, $S_{\theta zmn}$, S_{xzmn}, $S_{x\theta mn}$, D_{xmn}, $D_{\theta mn}$, D_{zmn}, P_{xmn}, $P_{\theta mn}$, P_{zmn}, Φ_{mn}, and T_{mn} are functions of z only. The following conditions are satisfied at $x = 0, L$,

$$v = w = \sigma_x = \phi = T = 0 \tag{9}$$

The electric potential, traction components, and temperature change at the inner and outer surfaces in Eq. (1) are also expanded in the double Fourier series as follows:

$$\{q_x^0, q_x^h\} = \sum_{m=0}\sum_{n=0}\{Q_{xmn}^0, Q_{xmn}^h\}\cos a_m x\cos n\theta$$

$$\{q_\theta^0, q_\theta^h\} = \sum_{m=1}\sum_{n=1}\{Q_{\theta mn}^0, Q_{\theta mn}^h\}\sin a_m x\sin n\theta \tag{10}$$

$$\{q_z^0, q_z^h\} = \sum_{m=1}\sum_{n=0}\{Q_{zmn}^0, Q_{zmn}^h\}\sin a_m x\cos n\theta$$

$$\{\phi^0, \phi^h\} = \sum_{m=1}\sum_{n=0}\{\Phi_{mn}^0, \Phi_{mn}^h\}\sin a_m x\cos n\theta$$
$$\{T^0, T^h\} = \sum_{m=1}\sum_{n=0}\{T_{mn}^0, T_{mn}^h\}\sin a_m x\cos n\theta \tag{11}$$

B. Response Analysis

1. *Governing Equations*

A mixed formulation is used with the fundamental unknowns consisting of the three displacement components; the three transverse stress components; the transverse component of the electric displacement field; electric potential; transverse heat-flux component; and temperature change. A state-space approach[18] is used to generate the thermoelectroelastic response of the shell. To simplify the equations, the vector of fundamental unknowns $\boldsymbol{R}^{(\eta)}$ [amplitudes of response quantities associated with a typical layer η and a typical pair of harmonics (m, n)] is defined as follows:

$$\boldsymbol{R}^{(\eta)}(z) = \left[\{U(z), V(z), W(z), \Phi(z), T(z), S_{\theta z}(z), S_{xz}(z), S_z(z), D_z(z), H_z(z)\}_{mn}^{(\eta)}\right]^T \tag{12}$$

where superscript T denotes matrix transposition.

The governing equations for each layer consist of 10 first-order ordinary differential equations as follows: four equilibrium equations, one gradient equation, and five constitutive relations (see Appendix A). For a typical layer, the governing equations, associated with a pair of harmonics (m, n), can be written as a vector–matrix differential equation as follows:

$$\boldsymbol{B}^{(\eta)}(z)\frac{\mathrm{d}}{\mathrm{d}z}\boldsymbol{R}^{(\eta)}(z) + \boldsymbol{A}^{(\eta)}(z) \qquad \boldsymbol{R}^{(\eta)}(z) = 0 \tag{13}$$

where the superscript η refers to the ηth layer and the system matrices $\boldsymbol{B}^{(\eta)}$ and $\boldsymbol{A}^{(\eta)}$ are

$$\boldsymbol{B}^{(\eta)}(z) = \boldsymbol{B}_0^{(\eta)} + \boldsymbol{B}_1^{(\eta)}z + \boldsymbol{B}_2^{(\eta)}z^2$$
$$\boldsymbol{A}^{(\eta)}(z) = \boldsymbol{A}_0^{(\eta)} + \boldsymbol{A}_1^{(\eta)}z + \boldsymbol{A}_2^{(\eta)}z^2 \tag{14}$$

The explicit form of the matrices $\boldsymbol{B}_i^{(\eta)}$ and $\boldsymbol{A}_i^{(\eta)}$ $(i = 0, 1, 2)$ are given in Appendix B.

The complete description of the plate response requires 1) the governing equations, Eq. (13), for each layer; 2) the stress equilibrium equations and the displacement compatibility relations at layer interfaces; and 3) the conditions at the inner and outer surfaces of the shell. The stress equilibrium and displacement compatibility conditions at the interface between the layers η and $(\eta + 1)$ [outer surface of layer η and inner surface of layer $(\eta + 1)$] can be written in the following form:

$$\boldsymbol{R}^{(\eta+1)}(0) = \boldsymbol{R}^{(\eta)}\left(h^{(\eta)}\right) \tag{15}$$

Equation (15) implies perfect bonding between the adjacent layers.

The boundary conditions at the inner and outer surfaces of the shell are expressed in terms of the components of the two vectors $\boldsymbol{R}^{(1)}(0)$ and $\boldsymbol{R}^{(N)}(h^{(N)})$, where

$$\boldsymbol{R}^{(1)}(0) = \left[\{U(0), V(0), W(0), \Phi(0), T(0), S_{\theta z}(0), S_{xz}(0), S_z(0), D_z(0), H_z(0)\}_{mn}^{(1)}\right]^T$$
$$\boldsymbol{R}^{(N)}\left(h^{(N)}\right) = \left[\left\{U\left(h^{(N)}\right), V\left(h^{(N)}\right), W\left(h^{(N)}\right), \Phi\left(h^{(N)}\right), T\left(h^{(N)}\right), S_{\theta z}\left(h^{(N)}\right), S_{xz}\left(h^{(N)}\right), S_z\left(h^{(N)}\right), D_z\left(h^{(N)}\right), H_z\left(h^{(N)}\right)\right\}_{mn}^{(N)}\right]^T \tag{16}$$

and N is the total number of layers. The quantities $S_{zmn}(0)$, $S_{\theta zmn}(0)$, $S_{xzmn}(0)$, $\Phi_{mn}(0)$, $T_{mn}(0)$, $S_{zmn}(h^{(N)})$, $S_{\theta zmn}(h^{(N)})$, $S_{xzmn}(h^{(N)})$, $\Phi_{mn}(h^{(N)})$, and $T_{mn}(h^{(N)})$ can be determined from the Fourier expansions of Eqs: (10) and (11).

2. Solutions

Equations (13) are simultaneous ordinary differential equations, with variable coefficients, in the response quantities. Closed-form solutions are not generally available. Series solution of Eq. (13) can be found by using the Frobenius method,[10] which has been successfully used to obtain solutions of elastic cylindrical shells. To apply this method to hybrid thermoelectroelastic shells, the solution of Eq. (13) is assumed to be of the form

$$\boldsymbol{R}_l^{(\eta)}(z) = \exp\left(s_l^{(\eta)} z\right) \sum_{k=0}^{\infty} \boldsymbol{u}_{kl}^{(\eta)} z^k \qquad l = 1, \ldots, 10 \tag{17}$$

where $s_l^{(\eta)}$ and $\boldsymbol{u}_{kl}^{(\eta)}$ are to be determined. If Eqs. (17) and (13) are used and the coefficients of z^k in the resulting equation disappear, the following recursive relation is obtained

$$\begin{aligned}\boldsymbol{u}_{(k+1)l}^{(\eta)} = -[1/(k+1)]\boldsymbol{B}_0^{(\eta)-1} \Big\{ &\left(s_l^{(\eta)}\boldsymbol{B}_0^{(\eta)} + \boldsymbol{A}_0^{(\eta)} + k\boldsymbol{B}_1^{(\eta)}\right)\boldsymbol{u}_{kl}^{(\eta)} \\ &+ \left[s\boldsymbol{B}_1^{(\eta)} + \boldsymbol{A}_1^{(\eta)} + (k-1)\boldsymbol{B}_2^{(\eta)}\right]\boldsymbol{u}_{(k-1)l}^{(\eta)} \\ &+ \left(s_l^{(\eta)}\boldsymbol{B}_2^{(\eta)} + \boldsymbol{A}_2^{(\eta)}\right)\boldsymbol{u}_{(k-2)l}^{(\eta)} \Big\}\end{aligned} \tag{18}$$

with $\boldsymbol{u}_{-2l}^{(\eta)} = \boldsymbol{u}_{-l}^{(\eta)} = \boldsymbol{u}_l^{(\eta)} = 0$ and the coefficients $s_l^{(\eta)}$ $(l = 1, \ldots, 10)$ are obtained from zeroth recursive equations in Eq. (18). The general solution for the ηth layer can be written in the following form:

$$\boldsymbol{R}^{(\eta)}(z) = \boldsymbol{F}^{(\eta)}(z)\boldsymbol{C} \tag{19}$$

where $\boldsymbol{C}$ is a constant vector and the transfer matrix $\boldsymbol{F}^{(\eta)}(z)$ is given by

$$\begin{aligned}\boldsymbol{F}^{(\eta)}(z) = \Bigg[&\exp\left(s_1^{(\eta)} z\right) \sum_{k=0}^{\infty} \boldsymbol{u}_{k1}^{(\eta)} z^k, \\ &\exp\left(s_2^{(\eta)} z\right) \sum_{k=0}^{\infty} \boldsymbol{u}_{k2}^{(\eta)} z^k, \ldots, \exp\left(s_{10}^{(\eta)} z\right) \sum_{k=0}^{\infty} \boldsymbol{u}_{k10}^{(\eta)} z^k \Bigg]\end{aligned} \tag{20}$$

If the initial state vector, associated with the inner surface of the ηth layer, is mapped into the state vector associated with the outer surface of the same layer and the interface conditions (16) are incorporated, the following relations are obtained:

$$\boldsymbol{R}^{(\xi)}(z) = \left[\prod_{\eta=1}^{\xi} \boldsymbol{F}^{(\eta)}(z)\boldsymbol{F}^{(\eta)-1}(0)\right]\boldsymbol{R}^{(1)}(0) \tag{21}$$

$$\boldsymbol{R}^{(N)}\left(h^{(N)}\right) = \left[\prod_{\eta=1}^{N} \boldsymbol{F}^{(\eta)}\left(h^{(\eta)}\right)\boldsymbol{F}^{(\eta)-1}(0)\right]\boldsymbol{R}^{(1)}(0) \tag{22}$$

Equation (22) constitutes a set of 10 simultaneous linear algebraic equations in the 10 unknown amplitudes $[U_{mn}(0), V_{mn}(0), W_{mn}(0), D_{\theta mn}(0), P_{\theta mn}(0), U_{mn}(h^{(N)}), V_{mn}(h^{(N)}), W_{mn}(h^{(N)}), D_{\theta mn}(h^{(N)})$, and $P_{\theta mn}(h^{(N)})]$ of the inner and outer surfaces of the shell. Once the response quantities associated with the inner and outer surfaces of the shell are obtained, the response quantities within each layer can be evaluated by using Eq. (21).

The in-plane components of the response quantities for the ηth layer are defined as follows:

$$\boldsymbol{T}^{(\eta)}(z) = \left[\{S_\theta(z), S_x(z), S_{\theta x}(z), D_\theta(z), D_x(z), P_\theta(z), P_x(z)\}_{mn}^{(\eta)}\right]^T$$

If the fundamental equations of three-dimensional thermoelectroelasticity are used (see Appendix A), the vector $\boldsymbol{T}^{(\eta)}$ can be expressed in terms of the vector $\boldsymbol{R}^{(\eta)}$ as follows:

$$\boldsymbol{T}^{(\eta)}(z) = \boldsymbol{M}^{(\eta)} \frac{\mathrm{d}}{\mathrm{d}z}\boldsymbol{R}^{(\eta)}(z) + \boldsymbol{H}^{(\eta)}\boldsymbol{R}^{(\eta)}(z) \tag{23}$$

where the explicit forms of the matrices $\boldsymbol{M}^{(\eta)}$ and $\boldsymbol{H}^{(\eta)}$ are given in Appendix B. After the response quantities in Eq. (21) and their derivatives in Eq. (13) have been obtained, the in-plane response vector $\boldsymbol{T}^{(\eta)}$ can be evaluated using Eq. (23).

The solutions in Eq. (13) also can be obtained by using the sublayer method, in which each layer is divided into sublayers and in each sublayer the system matrices $\boldsymbol{A}$ and $\boldsymbol{B}$ are assumed to be constant.[15] Then, the solutions mapping the boundary conditions on the inner and outer surfaces are

$$\boldsymbol{R}^{(MN)}\left(h^{(MN)}\right) = \left(\prod_{\eta=1}^{MN} \exp\left(\bar{\boldsymbol{A}}^{(\eta)} h^{(\eta)}\right)\right)\boldsymbol{R}^{(1)}(0) \tag{24}$$

where M is the number of sublayers, $\bar{\boldsymbol{A}}^{(\eta)} = \boldsymbol{B}^{(\eta)-1}(\bar{z})\,\boldsymbol{A}^{(\eta)}(\bar{z})$, and $\bar{z}$ is the value of z at the middle surface of the ηth sublayer. The exponential matrix $\exp(\bar{\boldsymbol{A}}^{(\eta)} h^{(\eta)})$ is the transfer matrix that maps the initial state vector, associated with the inner surface of the ηth layer into the state vector associated with the outer surface of the same layer. The response $\boldsymbol{R}^{(\eta)}$ and in-plane response $\boldsymbol{T}^{(\eta)}$ can be obtained by following similar steps as those used with Eqs. (21–23).

C. Sensitivity Analysis

Analytical sensitivity coefficients (derivatives of response quantities with respect to material, lamination, and geometric parameters of the shell) are used to study the sensitivity of the shell response to variations in the different shell parameters. The governing equations for the sensitivity coefficients of the response quantities are generated by differentiating Eq. (21) for the Frobenius method and Eq. (24) for the sublayer method. For the Frobenius method, the sensitivity equations for each pair of Fourier harmonics are

$$\begin{aligned}\boldsymbol{X}^{(\xi)}(z) = &\left[\prod_{\eta=1}^{\xi} \boldsymbol{F}^{(\eta)}(z)\boldsymbol{F}^{(\eta)-1}(0)\right]\boldsymbol{X}^{(1)}(0) \\ &+ \frac{\partial}{\partial\lambda}\left[\prod_{\eta=1}^{\xi} \boldsymbol{F}^{(\eta)}(z)\boldsymbol{F}^{(\eta)-1}(0)\right]\boldsymbol{R}^{(1)}(0)\end{aligned} \tag{25}$$

$$\begin{aligned}\boldsymbol{X}^{(N)}\left(h^{(N)}\right) = &\left[\prod_{\eta=1}^{N} \boldsymbol{F}^{(\eta)}\left(h^{(\eta)}\right)\boldsymbol{F}^{(\eta)-1}(0)\right]\boldsymbol{X}^{(1)}(0) \\ &+ \frac{\partial}{\partial\lambda}\left[\prod_{\eta=1}^{N} \boldsymbol{F}^{(\eta)}\left(h^{(\eta)}\right)\boldsymbol{F}^{(\eta)-1}(0)\right]\boldsymbol{R}^{(1)}(0)\end{aligned} \tag{26}$$

where $\boldsymbol{X}^{(\eta)}(z) = \partial\boldsymbol{R}^{(\eta)}(z)/\partial\lambda$, and λ is a typical material, lamination, or geometric parameter of the shell. The boundary conditions on the inner and outer surfaces are

$$\begin{aligned}&\boldsymbol{X}^{(1)}(0) \\ &= \frac{\partial}{\partial\lambda}\left[\{U(0), V(0), W(0), 0, 0, 0, 0, 0, D_\theta(0), H_\theta(0)\}_{mn}^{(1)}\right]^T\end{aligned} \tag{27}$$

$$\begin{aligned}\boldsymbol{X}^{(N)}\left(h^{(N)}\right) = \frac{\partial}{\partial\lambda}\Big[&\left\{U\left(h^{(N)}\right), V\left(h^{(N)}\right), W\left(h^{(N)}\right),\right. \\ &\left. 0, 0, 0, 0, 0, D_\theta\left(h^{(N)}\right), H_\theta\left(h^{(N)}\right)\right\}_{mn}^{(N)}\Big]^T\end{aligned}$$

Equation (26) is a set of 10 linear simultaneous algebraic equations associated with the amplitudes of the sensitivity coefficient:

$$\frac{\partial U_{mn}(0)}{\partial\lambda}, \quad \frac{\partial V_{mn}(0)}{\partial\lambda}, \quad \frac{\partial W_{mn}(0)}{\partial\lambda}, \quad \frac{\partial D_{\theta mn}(0)}{\partial\lambda}$$

$$\frac{\partial P_{\theta mn}(0)}{\partial\lambda}, \quad \frac{\partial U_{mn}(h^{(N)})}{\partial\lambda}, \quad \frac{\partial V_{mn}(h^{(N)})}{\partial\lambda}$$

$$\frac{\partial W_{mn}(h^{(N)})}{\partial\lambda}, \quad \frac{\partial D_{\theta mn}(h^{(N)})}{\partial\lambda}, \quad \frac{\partial P_{\theta mn}(h^{(N)})}{\partial\lambda}$$

of the inner and outer surfaces of the shell. Once the sensitivity coefficients on the inner and outer surfaces are obtained, the sensitivity coefficients within each layer are evaluated by using Eq. (25), and the in-plane sensitivity coefficients are obtained by differentiating Eq. (23) with respect to λ. The same procedure can be used to obtain the sensitivity coefficients of the response quantities for the sublayer approach.

D. Comments on the Computational Procedures

As the number of terms in Eq. (20) increases for the Frobenius method, or the number of sublayers increases in Eq. (24) for the sublayer method, the solution of the response quantities of the shell is expected to converge to the exact solution. In practice, only a finite number of terms in the Frobenius method, or a finite number of sublayers in the sublayer method, are used. To study the convergence of the Frobenius method, the transfer matrix with $K+1$ terms in the series for the ηth layer in Eq. (20) is evaluated:

$$\boldsymbol{F}_K(z) = \left[\exp(s_1 z) \sum_{k=0}^{K} \boldsymbol{u}_{k1} z^k, \right.$$

$$\left. \exp(s_2 z) \sum_{k=0}^{K} \boldsymbol{u}_{k2} z^k, \ldots, \exp(s_{10} z) \sum_{k=0}^{K} \boldsymbol{u}_{k10} z^k \right] \tag{28}$$

where the superscripts (η) are omitted for brevity. The following convergence criterion is used:

$$\left| \frac{\left\| \int_{h^{(\eta)}} \boldsymbol{F}_{K+1}(z)\, \mathrm{d}z \right\|_2 - \left\| \int_{h^{(\eta)}} \boldsymbol{F}_K(z)\, \mathrm{d}z \right\|_2}{\left\| \int_{h^{(\eta)}} \boldsymbol{F}_{K+1}(z)\, \mathrm{d}z \right\|_2} \right| < \varepsilon_1 \tag{29}$$

where $\|\cdot\|_2$ is the Euclidean norm and ε_1 is a prescribed tolerance.

For the sublayer method, the convergence is studied by examining the solutions of the surface response quantities in Eq. (24) (which depend on the number of sublayers in each layer). The solution vector with M sublayers in each layer of the shell can be written in the following form:

$$\boldsymbol{G}_M = \left\{ \left[U(0), V(0), W(0), D_z(0), H_z(0), U\left(h^{(N)}\right), V\left(h^{(N)}\right), \right.\right.$$

$$\left.\left. W\left(h^{(N)}\right), D_z\left(h^{(N)}\right), H_z\left(h^{(N)}\right) \right]^M \right\}^T \tag{30}$$

The following convergence criterion is used:

$$\left| \frac{\|\boldsymbol{G}_{M+1}\|_2 - \|\boldsymbol{G}_M\|_2}{\|\boldsymbol{G}_{M+1}\|_2} \right| < \varepsilon_2 \tag{31}$$

where ε_2 is a prescribed tolerance.

Note that Eqs. (13) and (22) or Eqs. (13) and (24) used in the response analysis represent a homogeneous two-point boundary-value problem. By contrast, Eq. (26) used in the sensitivity analysis represents a nonhomogeneous two-point boundary value problem, and the forcing terms are dependent on the solutions for the response quantities.[18] The eigen derivative theory[19] is used to evaluate the sensitivity of the recursive relation, Eq. (18).

If the distributions of the electrical and thermal fields in the thickness direction are known, then the coupled governing differential equations reduce to six decoupled first-order nonhomogeneous ordinary differential equations, with the fundamental unknowns consisting of three displacement components and three transverse stress components. The elastic response of the shell can be obtained by solving the nonhomogeneous two-point boundary-value problem. The decoupled case has been presented in the literature.[4–10]

The aforementioned solutions for the responses and sensitivity coefficients can be generalized to simply-supported cylindrical panels by replacing the trigonometric functions $\cos(n\theta)$ and $\sin(n\theta)$ in Eqs. (2–6) and Eqs. (10) and (11) by $\sin(b_n\theta)$ and $\cos(b_n\theta)$, respectively, where $b_n = n\pi/\Theta$ and Θ is the total subtended angle of the panel, and by assuming that the boundary conditions $u = w = \sigma_\theta = \phi = T = 0$ at $\theta = 0$ and Θ are satisfied.

III. Numerical Studies

To assess the effects of variations in the material characteristics of the individual layers on the steady-state response, several problems

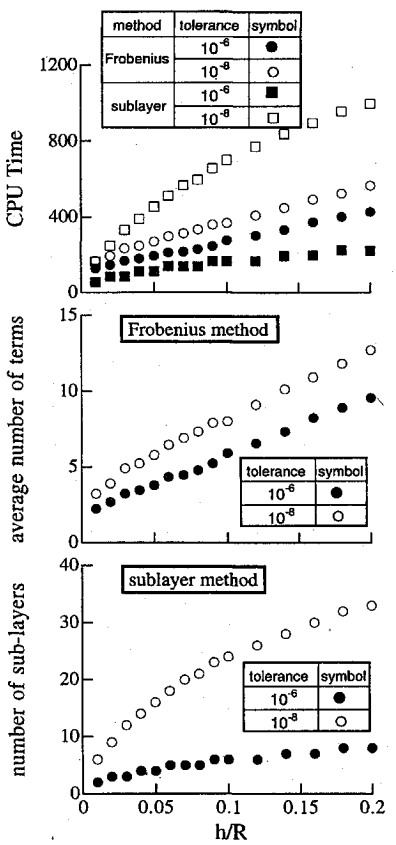

Fig. 2 Effect of thickness ratio on CPU time and convergence of the solutions obtained by the Frobenius and the sublayer methods, for hybrid multilayered shells [configuration (a)] subjected to mechanical load.

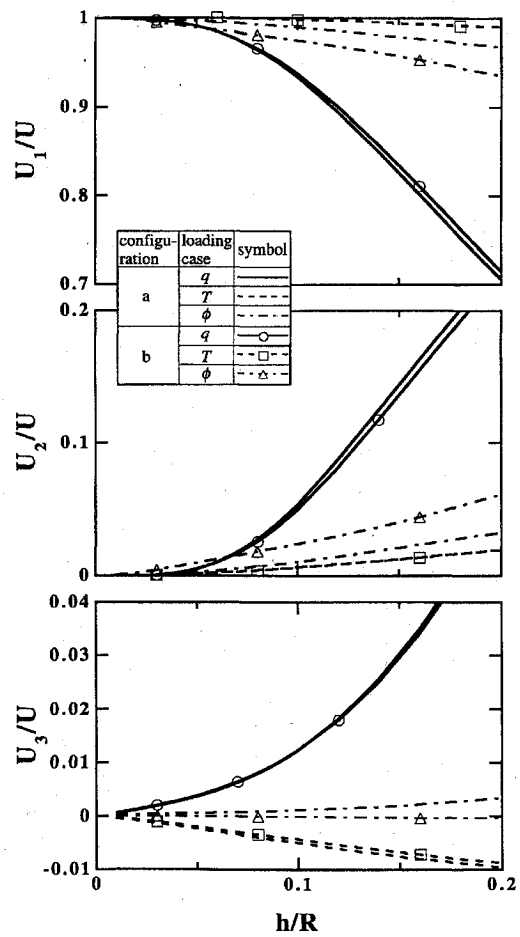

Fig. 3 Effect of thickness ratio on strain-energy ratios, for hybrid multilayered shells [configurations (a) and (b)] subjected to mechanical load, temperature change, and electric potential.

of hybrid composite cylindrical shells are solved. The shells are subjected to mechanical, thermal, and electric loading. For each problem the derivatives of the response quantities with respect to the different material parameters are evaluated. Both the Frobenius method and the sublayer method are used to obtain all the response quantities and their sensitivity coefficients. The solutions presented provide an insight into the effect of the thermoelectroelastic layers on the response of the shells. They also can help assess the reliability of various two-dimensional theories for predicting the steady-state response and its sensitivity to variations in the material and lamination parameters of the shell.

The shells considered are made of eight graphite–epoxy layers with fiber orientation $(0/90\ \text{deg})_4$, with fibers of the outer layer in the x direction. The radius of the middle surface and the length of the shell are selected to be $R = 1$ and $L = 1$, respectively. Two different shell configurations are analyzed: one has a single PZT-5A piezoelectric layer at the outer surface [configuration (a)] and the other at the mid-thickness [configuration (b)] (see Fig. 1). The layers of the two shell configurations are of equal thickness and are perfectly bonded together. The material properties of the graphite–epoxy and the PZT-5A layer are given in Table 1. Three different loadings are applied to the inner surface of the shell: transverse mechanical loading $q_z^0 = q_0 \sin a_1 x \sin 2\theta$, temperature change $T^0 = T_0 \sin a_1 x \sin 2\theta$, and electric potential $\phi^0 = \phi_0 \sin a_1 x \sin 2\theta$. The three loadings have unit amplitude ($q_0 = T_0 = \phi_0 = 1$). Henceforth, for brevity, the three loading cases will be referred to as q-case, T-case, and ϕ-case, respectively. The thickness ratio h/R was varied between 0.01 and 0.2.

To assess the importance of the transverse stresses $\{\tau_{xz}, \tau_{\theta z}, \sigma_z\}$ on the response of the shell, the total strain energy U was decomposed into three components: in-plane component U_1 associated with the stresses $\{\sigma_x, \sigma_\theta, \tau_{x\theta}\}$ and strains $\{\varepsilon_x^E, \varepsilon_\theta^E, \gamma_{x\theta}^E\}$, transverse shear component U_2 associated with the stresses $\{\tau_{xz}, \tau_{\theta z}\}$ and strains $\{\gamma_{xz}^E, \gamma_{\theta z}^E\}$, and transverse normal stress/strain component U_3 associated with the stress component σ_z and the strain component ε_z^E, where $\{\varepsilon_x^E, \varepsilon_\theta^E, \varepsilon_z^E, \gamma_{\theta z}^E, \gamma_{xz}^E, \gamma_{x\theta}^E\}$ are the mechanical parts of the total strain components; and the total strain energy U is $U = U_1 + U_2 + U_3$.

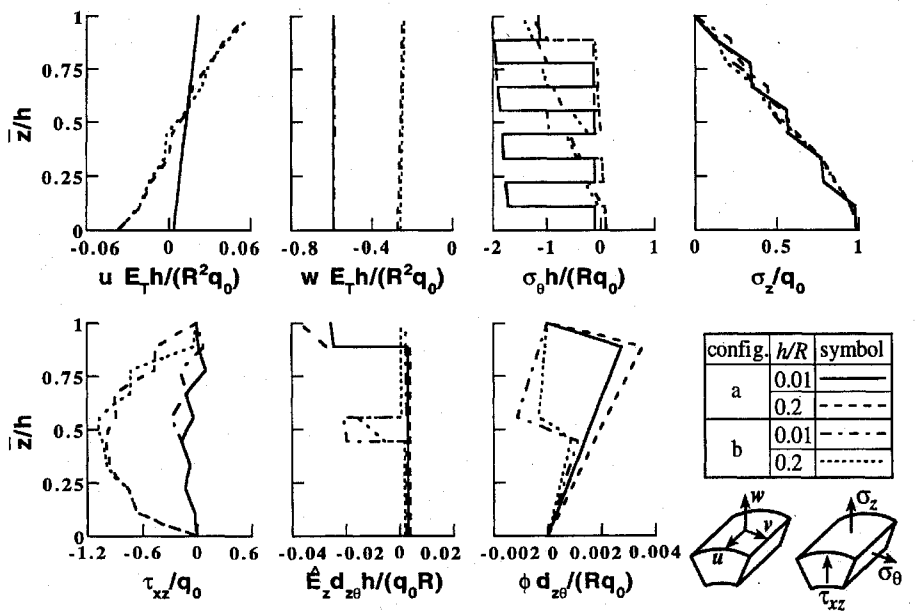

Fig. 4 Through-the-thickness variations of the displacements, stresses, electric field, and electric potential for hybrid multilayered shells subjected to mechanical load [configurations (a) and (b), $h/L = 0.01$, 0.2, and $q_0 = 1$].

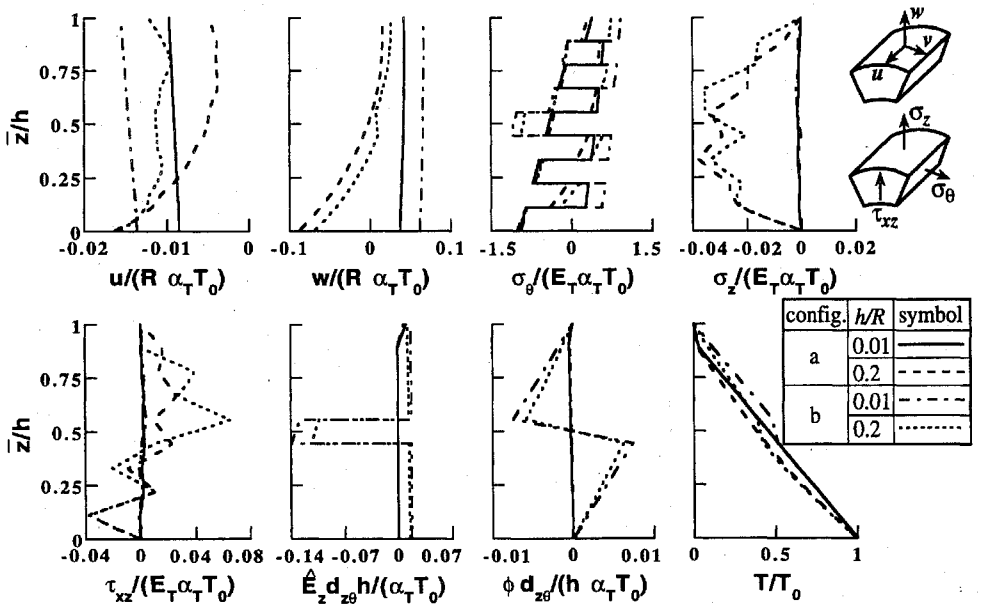

Fig. 5 Through-the-thickness variations of the displacements, stresses, electric field, electric potential, and temperature change for hybrid multilayered shells subjected to temperature change [configurations (a) and (b), $h/L = 0.01$, 0.2, and $T_0 = 1$].

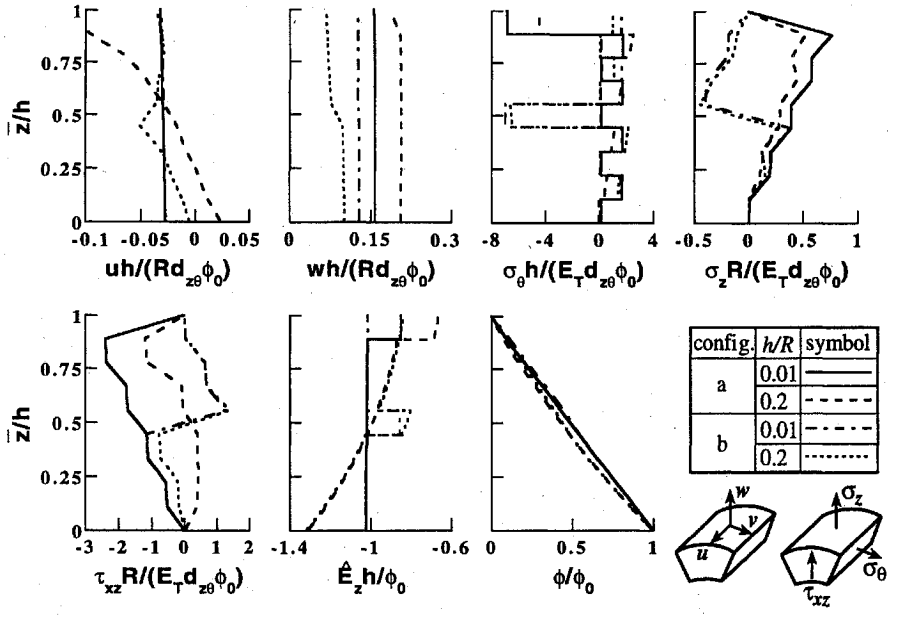

Fig. 6 Through-the-thickness variations of the displacements, stresses, electric field, and electric potential for hybrid multilayered shells subjected to electric potential [configurations (a) and (b), $h/L = 0.01, 0.2$, and $\phi_0 = 1$].

Table 1 Material properties of the graphite–epoxy and PZT-5A layers used in the present study

Graphite–epoxy layer		PZT-5A layer	
Property	Value	Property	Value
E_L (10^9 Pa)	181	E_x (10^9 Pa)	61.0
E_T (10^9 Pa)	10.3	E_θ (10^9 Pa)	61.0
		E_z (10^9 Pa)	53.2
G_{LT} (10^9 Pa)	7.17	$G_{x\theta}$ (10^9 Pa)	22.6
		$G_{\theta z}$ (10^9 Pa)	21.1
G_{TT} (10^9 Pa)	2.87	G_{xz} (10^9 Pa)	21.1
υ_{LT}	0.28	$\upsilon_{x\theta}$	0.35
		$\upsilon_{\theta z}$	0.38
υ_{TT}	0.33	υ_{xz}	0.38
α_L (10^{-6}/°C)	0.02	α_x (10^{-6}/°C)	1.5
α_T (10^{-6}/°C)	22.5	α_θ (10^{-6}/°C)	1.5
	22.5	α_z (10^{-6}/°C)	2.0
k_L (W/m°C)	1.5	k_x (W/m°C)	1.8
k_T (W/m°C)	0.5	k_θ (W/m°C)	1.8
		k_z (W/m°C)	1.8
d_{zx} (10^{-12} m/V)	0	d_{zx} (10^{-12} m/V)	−171
$d_{z\theta}$ (10^{-12} m/V)	0	$d_{z\theta}$ (10^{-12} m/V)	−171
d_{zz} (10^{-12} m/V)	0	d_{zz} (10^{-12} m/V)	374
d_{xxz} (10^{-12} m/V)	0	d_{xxz} (10^{-12} m/V)	584
$d_{\theta\theta z}$ (10^{-12} m/V)	0	$d_{\theta\theta z}$ (10^{-12} m/V)	584
κ_x (10^{-8} F/m)	1.53	κ_x (10^{-8} F/m)	1.53
κ_θ (10^{-8} F/m)	1.53	κ_θ (10^{-8} F/m)	1.53
κ_z (10^{-8} F/m)	1.53	κ_z (10^{-8} F/m)	1.50
$\hat{r}_z$ (C/m^2)	0	$\hat{r}_z$ (C/m^2)	0.0007

The numerical solutions presented were subsequently performed using the Mathematica system on the SunSPARC 10 workstation with operating system SunOS 4.1.3.

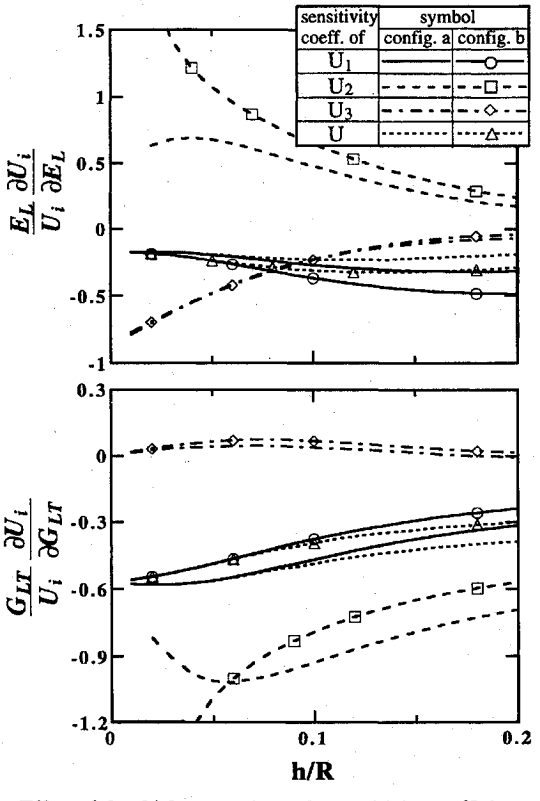

Fig. 7 Effect of the thickness ratio on the sensitivity coefficients of the strain-energy components U_1, U_2, U_3, and the total strain energy U, with respect to material properties E_L and G_{LT}, for hybrid multilayered shells subjected to mechanical load [configurations (a) and (b)].

A. Response Analysis

An indication of the convergence of the solutions obtained by both the Frobenius and the sublayer methods with the thickness ratio is given in Fig. 2 for the case of the mechanical loading and shell configuration (a). For the other configuration and the other loading cases, numerical experiments show similar convergence trends. Figure 2 shows that the CPU time expended in both the Frobenius and the sublayer methods depends on the tolerances ε_1 and ε_2. For smaller tolerance, the CPU time expended in the sublayer method is higher than that in the Frobenius method. The CPU time for both methods also increases with the increase in the thickness ratio. The average number of terms needed for convergence in the Frobenius method is also shown in Fig. 2. The number of terms increases with the increase in the thickness ratio. For a prescribed tolerance $\varepsilon_1 = 10^{-6}$ and $h/R = 0.2$, the average number of the terms is 9. For the sublayer method, the number of the sublayers needed for convergence increases with the increase in the thickness ratio, as shown in Fig. 2. For a prescribed tolerance of $\varepsilon_2 = 10^{-6}$, the number of sublayers is 8. In the solutions discussed, the Frobenius method is used, and the prescribed tolerance $\varepsilon_1 = 10^{-8}$.

Typical results for the three loading cases and the two shell configurations are shown in Figs. 3–6. The variations of the strain-energy

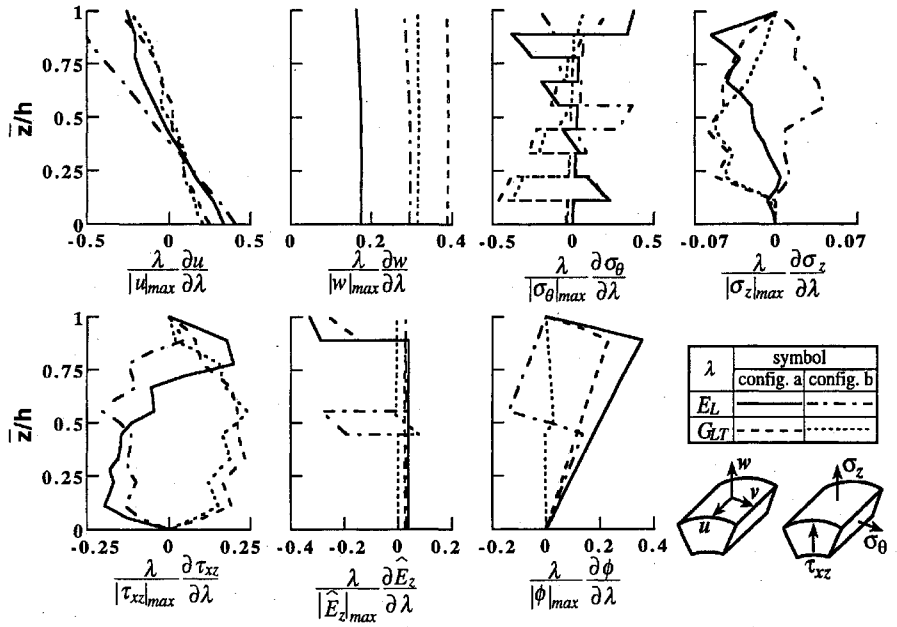

Fig. 8 Through-the-thickness variations of the sensitivity coefficients of the displacements, stresses, electric field, and electric potential, with respect to material properties E_L and G_{LT}, for hybrid multilayered shells subjected to mechanical load [configurations (a) and (b), $h/L = 0.2$].

components with the thickness ratio of the shell are shown in Fig. 3. The thickness distributions of the displacement components u, w, stress components σ_θ, σ_z, τ_{xz}, electric field component $\hat{E}_z$, electric potential ϕ, and temperature change T for the shells with $h/R = 0.01$ and 0.2 are shown in Figs. 4–6, in which the thickness coordinate $\bar{z}$ is used [see Fig. 1 ($0 \leq \bar{z} \leq h$)].

An examination of Figs. 3–6 reveals the following:

1) As expected, the in-plane strain-energy ratio U_1/U decreases with the increase in the thickness ratio of the shell. The decrease in U_1/U is associated with an increase in the transverse-shear strain-energy ratio, U_2/U. However, only for the q-case, the ratio U_2/U exhibits a pronounced change with the change in the thickness ratio h/R. For the T- and ϕ-cases, the ratio U_2/U is small compared with U_2/U for the q-case. The transverse-normal strain-energy ratio U_3/U is one order of magnitude smaller than the transverse-shear strain-energy ratio U_2/U and is negative for the T-case.

2) For the q-case and the T-case, the energy ratios for configurations (a) and (b) are almost the same. However, the energy ratios for the ϕ-case associated with the two shell configurations are significantly different. The difference between the corresponding energy ratios increases with the increase in the thickness ratio.

3) When the thickness ratio of the shell is small ($h/R = 0.01$), the thickness distributions of the displacement components u and w are nearly linear and uniform, respectively (for both configurations and for the three loading cases). However, when the thickness ratio is large (e.g., $h/R = 0.2$), the distributions of u and w in the thickness direction are nonlinear. The nonlinearity is more pronounced for the T- and ϕ-cases than for the q-case.

4) For the T-case and the ϕ-case, the presence of the piezoelectric layer at the midthickness of the shell leads to significantly different distributions of the various response quantities from the case when the piezoelectric layer is at the outer surface. This is particularly true for thick shells with $h/R = 0.2$. For the q-case, the effect of the location of the piezoelectric layer on the distribution of the different response quantities is not significant. Exceptions to that are the electric-response quantities, which are strongly affected by the location of the piezoelectric layer.

5) For the T-case and the ϕ-case, the transverse stress components τ_{xz} and σ_z are small, compared with the in-plane stress component σ_θ. This explains dominance of the in-plane strain energy U_1, for the T-case and the ϕ-case, even when the displacement components have a pronounced nonlinear distribution through the thickness.

6) The distribution of the temperature in the thickness direction is significantly affected by both the presence and the location of the piezoelectric layer. This is true even for thin shells [with h/R of $\mathcal{O}(0.01)$].

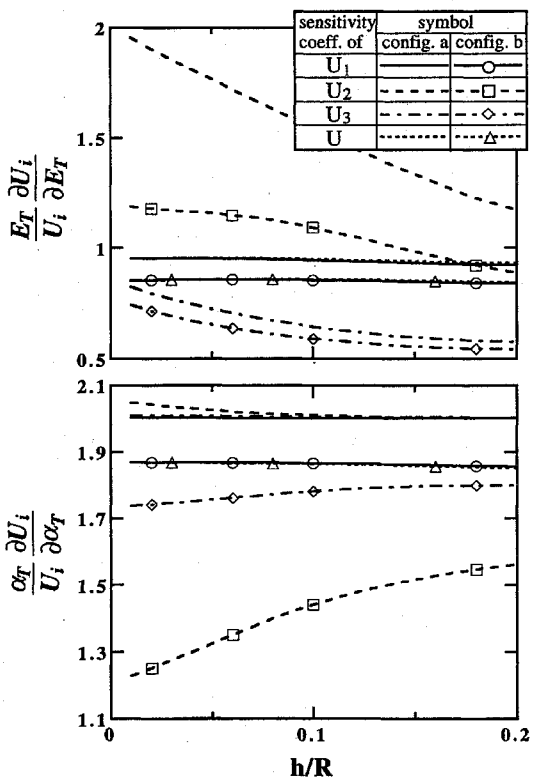

Fig. 9 Effect of the thickness ratio on the sensitivity coefficients of the strain-energy components U_1, U_2, U_3, and the total strain-energy U, with respect to material properties E_T and α_T, for hybrid multilayered shells subjected to temperature change [configurations (a) and (b)].

B. Sensitivity Analysis

A sensitivity study is conducted to assess the sensitivity of the different response quantities to variations in the different material parameters of the shell. Typical results are shown in Figs. 7–12. Based on the numerical studies conducted, the dominant sensitivity coefficients of the total strain energy are those with respect to

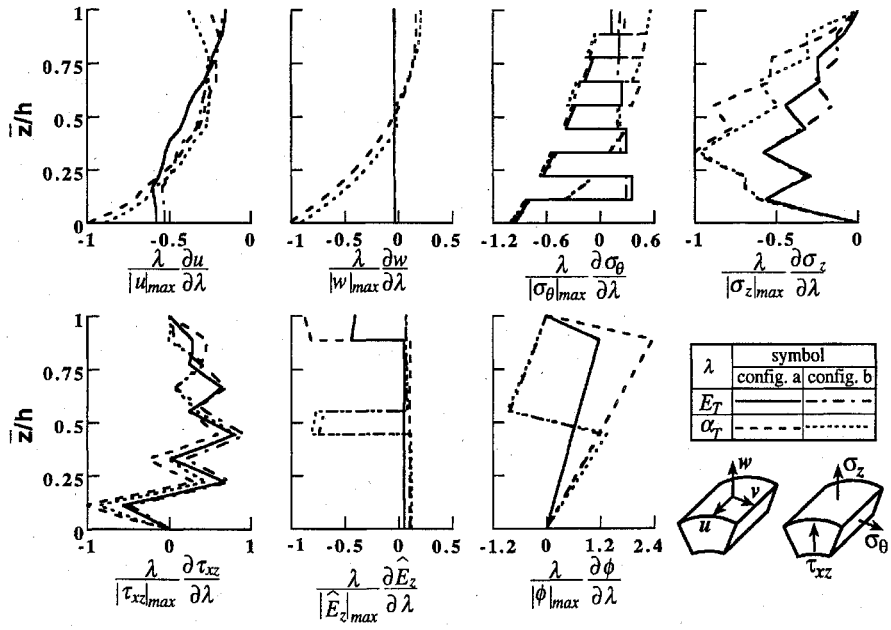

Fig. 10 Through-the-thickness variations of the sensitivity coefficients of the displacements, stresses, electric field, and electric potential, with respect to material properties E_T and α_T, for hybrid multilayered shells subjected to temperature change [configurations (a) and (b), $h/L = 0.2$].

Young's modulus E_L and shear modulus G_{LT} of the graphite–epoxy layers, for q-case; Young's modulus E_T and thermal expansion coefficient α_T of the graphite–epoxy layers, for T-case; and the piezoelectric coefficient $d_{z\theta}$ and dielectric coefficient κ_z of the PZT-5A layer, for ϕ-case. The subscripts L and T denote fiber and transverse directions, respectively. The effects of variations in h/R on the sensitivity coefficients of U_i ($i = 1, 2, 3$) and U are shown in Figs. 7, 9, and 11 for the three loading cases. Each sensitivity coefficient is normalized by multiplying it by the associated material parameter and dividing by U_i (or U). The thickness distributions of the sensitivity coefficients of u, w, σ_θ, τ_{xz}, σ_z, $\hat{E}_z$, and ϕ are shown in Figs. 8, 10, and 12 for the three loading cases for shells with $h/R = 0.2$. In Figs. 8, 10, and 12, the thickness coordinate $\bar{z}$ is used. Each sensitivity coefficient is normalized by multiplying it by the associated material parameter and dividing by the maximum absolute value of the response quantity.

An examination of Figs. 7–12 reveals the following:

1) For the q-case, the strain-energy component U_2 is more sensitive to variations in the material parameters than the other energy components. For the T-case, the sensitivity of U_2 is more pronounced for shell configuration (a). For the ϕ-case, the strain-energy component U_1 is more sensitive to variations in the material parameters than the other energy components. For both the T-case and the ϕ-case, the strain-energy component U_3 is less sensitive to variations in the material parameters than are U_1 and U_2.

2) For both the T-case and the ϕ-case, the normalized sensitivity coefficients of U_1 are almost equal to that of U. For the q-case, the normalized sensitivity coefficients of U_1 are nearly equal to that of U for small values of h/R. As h/R increases, the difference between the two sensitivity coefficients increases.

3) For shell configuration (a), the normalized sensitivity coefficients of all the energy components with respect to the material parameters are nearly equal for the ϕ-case. However, for shell configuration (b), the normalized sensitivity coefficients of all of the energy components with respect to the material parameters are significantly different. The normalized sensitivity coefficients of the energy components U_1 and U_3 for shell configurations (a) and (b) for q-case have similar trends.

4) For the ϕ-case, the normalized sensitivity coefficients of the energy components for shell configuration (a) are insensitive to variations in h/R. This is also true for the normalized sensitivity coefficients of the energy components with respect to α_T in configuration (a) for the T-case.

5) For all the loading cases considered, the distribution of the sensitivity coefficients of the displacement component u in the thickness direction is highly nonlinear. The thickness distributions of $\partial w/\partial E_L$ and $\partial w/\partial G_{LT}$ for the q-case, and $\partial w/\partial E_T$ for the T-case in the thickness direction are almost uniform. On the other hand, the distribution of $\partial w/\partial \alpha_T$ for the T-case is nonlinear. For the ϕ-case, the distribution of the sensitivity coefficients of the displacement components in the thickness direction is significantly affected by the location of the thermoelectroelastic layer.

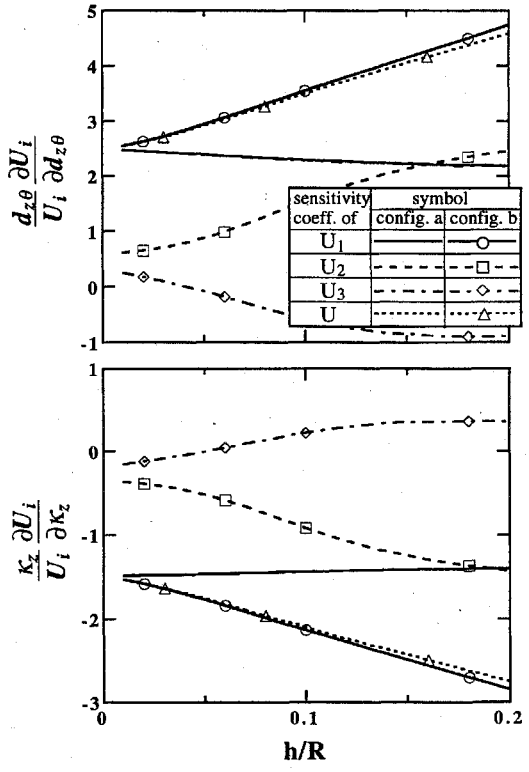

Fig. 11 Effect of thickness ratio on sensitivity coefficients of the strain-energy components U_1, U_2, U_3, and the total strain energy U, with respect to material properties d_{31} and κ_{33}, for hybrid multilayered shells subjected to electric potential [configurations (a) and (b)].

6) The thickness distributions of the sensitivity coefficients of the stress component σ_θ are almost piecewise linear. The thickness distributions of the sensitivity coefficients of the stress components

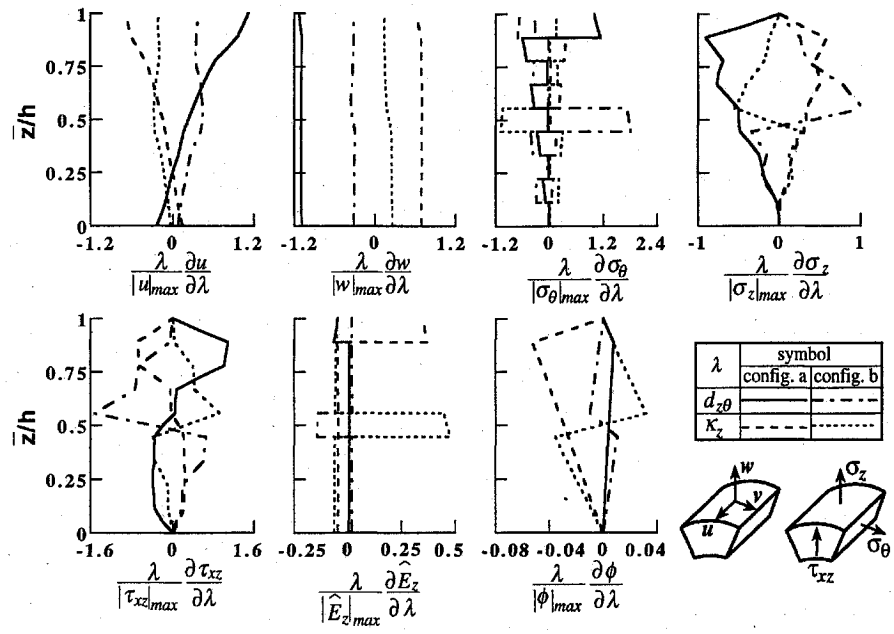

Fig. 12 Through-the-thickness variations of the sensitivity coefficients of the displacements, stresses, electric field, and electric potential, with respect to material properties d_{31} and κ_{33}, for hybrid multilayered shells subjected to electric potential [configurations (a) and (b), $h/L = 0.2$].

σ_z and τ_{xz} are piecewise continuous. The sensitivity coefficients of both σ_z and τ_{xz} are zero at the inner and outer surfaces of the shells.

7) A sharp change in the thickness distributions of the sensitivity coefficients of ϕ occurs at the location of the thermoelectroelastic layer. Consequently, the maximum value of the sensitivity coefficients of $\hat{E}_z$ occurs at the location of the thermoelectroelastic layer.

IV. Concluding Remarks

Analytical three-dimensional solutions are presented for the fully coupled thermoelectroelastic response of hybrid multilayered composite cylindrical shells. The sensitivity coefficients also are evaluated and are used to study the sensitivity of the different response quantities to variations in material parameters of the shells. The shells are made of perfectly bonded thermoelectroelastic and fiber-reinforced layers, subjected to mechanical loading, temperature change, and electric potential at the inner and outer surfaces. The linear three-dimensional fully coupled theory of thermoelectroelastic solids is used in this study.

Each of the response quantities of the shell is expanded in a double Fourier series in the local surface coordinates. A state-space approach is used to generate the response of the plate using 10 first-order ordinary homogeneous differential equations with variable coefficients. The solutions are obtained by either a modified Frobenius method or by the sublayer method. The efficiency of both methods is dependent on the tolerance specified. The sensitivity coefficients of the responses are obtained by direct differentiation of the governing equations of the response quantities.

Numerical results are presented for closed cylindrical shells made of eight graphite–epoxy layers and one PZT-5A layer at either the outer surface or the midthickness. The results show the effects of the thickness ratios and the location of the thermoelectroelastic layer on both the response quantities and the sensitivity coefficients, for mechanical loading, temperature change, and electric potential. The results presented give an insight into the differences between the response quantities, and their sensitivity coefficients, for the mechanical loading, temperature change, and electric potential. They also can help to assess the accuracy and range of validity of two-dimensional models for hybrid shells consisting of fiber-reinforced and thermoelectroelastic layers.

Acknowledgments

The present work is supported by NASA Cooperative Agreement NCCW-0011. The authors acknowledge useful discussions with W. Scott Burton of the Center for Computational Structures Technology, and Samuel L. Venneri of NASA Headquarters. The material properties for PZT-5A used in the present study were obtained from Morgan Matroc, Inc.

Appendix A: Fundamental Equations of Three-Dimensional Thermoelectroelasticity Theory

The equations governing the static linear response of a thermoelectroelastic medium can be grouped into three sets of equations in the cylindrical coordinate system $\{x, \theta, r\}$, namely, gradient relations, equilibrium equations, and constitutive relations, as follows:

Gradient relations

$$\varepsilon_x = \frac{\partial u}{\partial x}, \qquad \varepsilon_\theta = \frac{1}{r}\left(\frac{\partial v}{\partial \theta} + w\right), \qquad \varepsilon_r = \frac{\partial w}{\partial r}$$

$$\gamma_{x\theta} = \frac{1}{r}\frac{\partial u}{\partial \theta} + \frac{\partial v}{\partial x}, \qquad \gamma_{\theta r} = \frac{1}{r}\frac{\partial w}{\partial \theta} + r\frac{\partial}{\partial r}\left(\frac{v}{r}\right) \tag{A1}$$

$$\gamma_{xr} = \frac{\partial u}{\partial r} + \frac{\partial w}{\partial x}$$

$$\hat{E}_x = -\frac{\partial \phi}{\partial x}, \qquad \hat{E}_\theta = -\frac{1}{r}\frac{\partial \phi}{\partial \theta}, \qquad \hat{E}_r = -\frac{\partial \phi}{\partial r} \tag{A2}$$

$$p_x = -k_y\frac{\partial T}{\partial x}, \qquad p_\theta = -\frac{k_\theta}{r}\frac{\partial T}{\partial \theta}, \qquad p_r = -k_r\frac{\partial T}{\partial r} \tag{A3}$$

Equilibrium equations

$$\frac{\partial \sigma_x}{\partial x} + \frac{\partial \tau_{x\theta}}{r\partial \theta} + \frac{1}{r}\frac{\partial}{\partial r}(r\tau_{xr}) = 0$$

$$\frac{\partial \tau_{x\theta}}{\partial x} + \frac{\partial \sigma_\theta}{r\partial \theta} + \frac{1}{r^2}\frac{\partial}{\partial r}(r^2\tau_{\theta r}) = 0 \tag{A4}$$

$$\frac{\partial \tau_{rx}}{\partial x} + \frac{\partial \tau_{r\theta}}{r\partial \theta} + \frac{\partial \sigma_r}{\partial r} + \frac{\sigma_r - \sigma_\theta}{r} = 0$$

$$\frac{\partial d_x}{\partial x} + \frac{\partial d_\theta}{r\partial \theta} + \frac{\partial d_r}{\partial r} = 0 \tag{A5}$$

$$\frac{\partial p_x}{\partial x} + \frac{\partial p_\theta}{r\partial \theta} + \frac{\partial p_r}{\partial r} = 0 \tag{A6}$$

Constitutive relations for orthorhombic materials with crystal class 2mm

$$\begin{aligned}
\sigma_x &= c_{xx}\varepsilon_x + c_{x\theta}\varepsilon_\theta + c_{xr}\varepsilon_r + e_{rx}\hat{E}_r + \lambda_x T \\
\sigma_\theta &= c_{x\theta}\varepsilon_x + c_{\theta\theta}\varepsilon_\theta + c_{\theta r}\varepsilon_r + e_{r\theta}\hat{E}_r + \lambda_\theta T \\
\sigma_r &= c_{xr}\varepsilon_x + c_{\theta r}\varepsilon_\theta + c_{rr}\varepsilon_r + e_{rr}\hat{E}_r + \lambda_r T \qquad \text{(A7)} \\
\tau_{xr} &= G_{xr}\gamma_{xr} + e_{xxr}\hat{E}_x, \qquad \tau_{\theta r} = G_{\theta r}\gamma_{\theta r} + e_{\theta\theta r}\hat{E}_\theta \\
\tau_{x\theta} &= G_{x\theta}\gamma_{x\theta}
\end{aligned}$$

$$\begin{aligned}
d_x &= e_{xxr}\gamma_{xr} + \kappa_x\hat{E}_x, \qquad d_\theta = e_{\theta\theta r}\gamma_{\theta r} + \kappa_\theta\hat{E}_\theta \\
d_r &= e_{rx}\varepsilon_x + e_{r\theta}\varepsilon_\theta + e_{rr}\varepsilon_r + \kappa_r\hat{E}_r + \hat{r}_r T
\end{aligned} \qquad \text{(A8)}$$

In Eqs. (A1–A8), $\{\sigma_x, \sigma_\theta, \sigma_r, \tau_{\theta r}, \tau_{xr}, \tau_{x\theta}\}$, $\{\varepsilon_x, \varepsilon_\theta, \varepsilon_r, \gamma_{\theta r}, \gamma_{xr}, \gamma_{x\theta}\}$, and $\{u_x, u_\theta, u_r\}$ denote the stress, strain, and displacement components, respectively; $\{d_x, d_\theta, d_r\}$, $\{\hat{E}_x, \hat{E}_\theta, \hat{E}_r\}$, and $\{p_x, p_\theta, p_r\}$ are the electric displacement, the electric field, and heat-flux components, respectively; ϕ is the electric potential; T is the temperature change; $\{c_{xx}, c_{x\theta}, c_{xr}, c_{\theta\theta}, c_{\theta r}, c_{rr}, G_{\theta r}, G_{xr}, G_{x\theta}\}$ are material stiffness coefficients; $\{e_{rx}, e_{r\theta}, e_{rr}, e_{\theta\theta r}, e_{xxr}\}$ are piezoelectric coefficients; $\{k_x, k_\theta, k_r\}$ are thermal conductivity coefficients; $\{\lambda_x, \lambda_\theta, \lambda_r\}$ are stress–temperature; $\{\kappa_x, \kappa_\theta, \kappa_r\}$ are permittivities; and $\hat{r}_r$ is the pyroelectric coefficient.

To obtain the governing equations in the surface coordinate system of Fig. 1, the variables x, θ, and r in Eqs. (A1–A8) are replaced by x, θ, and $r_\eta + z$, respectively, where r_η is the radius of the inner surface of ηth layer (see Fig. 1). The origin of the surface coordinate system is selected to be at the inner surface of the ηth layer. For convenience, the subscript r used with the material coefficients in Eqs. (A7) and (A8) is replaced by the subscript z.

Appendix B: Explicit Form of the Matrices in Eqs. (14) and (23)

In the following matrices, the material parameters are given according to the orthogonal-shell-surface coordinate system $\{x, \theta, z\}$. For a typical layer η, $\boldsymbol{B}_i^{(\eta)}$, and $\boldsymbol{A}_i^{(\eta)}$ $(i = 0, 1, 2)$ in Eq. (14) are

$$\boldsymbol{B}_0^{(\eta)} = \begin{bmatrix}
r_\eta & 0 & 0 & 0 & 0 & 0 & 0 & 0 & 0 & 0 \\
0 & 1 & 0 & 0 & 0 & 0 & 0 & 0 & 0 & 0 \\
0 & 0 & r_\eta & 0 & 0 & 0 & 0 & 0 & 0 & 0 \\
0 & 0 & 0 & r_\eta & 0 & 0 & 0 & 0 & 0 & 0 \\
0 & 0 & 0 & 0 & 1 & 0 & 0 & 0 & 0 & 0 \\
0 & 0 & 0 & 0 & 0 & r_\eta^2 & 0 & 0 & 0 & 0 \\
0 & 0 & 0 & 0 & 0 & 0 & r_\eta^2 & 0 & 0 & 0 \\
0 & 0 & 0 & 0 & 0 & 0 & 0 & r_\eta^2 & 0 & 0 \\
b_{91} & b_{92} & 0 & 0 & 0 & 0 & 0 & 0 & r_\eta^2 & 0 \\
0 & 0 & 0 & 0 & 0 & 0 & 0 & 0 & 0 & r_\eta^2
\end{bmatrix}$$

$$\boldsymbol{B}_1^{(\eta)} = \frac{\mathrm{d}\boldsymbol{B}_0^{(\eta)}}{\mathrm{d}r_\eta}, \qquad \boldsymbol{B}_2^{(\eta)} = \frac{\mathrm{d}^2\boldsymbol{B}_0^{(\eta)}}{2\,\mathrm{d}r_\eta^2}$$

$$\boldsymbol{A}_0^{(\eta)} = \begin{bmatrix}
-1 & 0 & -b_n & a_{14} & 0 & a_{16} & 0 & 0 & 0 & 0 \\
0 & 0 & a_m & a_{24} & 0 & 0 & a_{27} & 0 & 0 & 0 \\
a_{31} & a_{32} & a_{33} & 0 & a_{35} & 0 & 0 & a_{38} & a_{39} & 0 \\
a_{41} & a_{42} & a_{43} & 0 & a_{45} & 0 & 0 & a_{48} & a_{49} & 0 \\
0 & 0 & 0 & 0 & 0 & 0 & 0 & 0 & 0 & 1/k_z \\
a_{61} & a_{62} & a_{63} & 0 & a_{65} & 2r_\eta & 0 & a_{68} & a_{69} & 0 \\
a_{62} & a_{72} & a_{73} & 0 & a_{75} & 0 & r_\eta & a_{78} & a_{79} & 0 \\
a_{63} & a_{73} & a_{83} & 0 & a_{85} & b_n r_\eta & -a_m r_\eta^2 & a_{88} & a_{89} & 0 \\
a_{91} & 0 & a_{93} & a_{94} & 0 & 0 & 0 & 0 & r_\eta & 0 \\
0 & 0 & 0 & 0 & a_{10,5} & 0 & 0 & 0 & 0 & r_\eta
\end{bmatrix}$$

$$\boldsymbol{A}_1^{(\eta)} = \frac{\mathrm{d}\boldsymbol{A}_0^{(\eta)}}{\mathrm{d}r_\eta}, \qquad \boldsymbol{A}_2^{(\eta)} = \frac{\mathrm{d}^2\boldsymbol{A}_0^{(\eta)}}{2\,\mathrm{d}r_\eta^2}$$

The a_{ij} and b_{ij} coefficients are given by

$$\begin{aligned}
b_{91} &= r_\eta b_n g_1, \qquad b_{92} = -r_\eta^2 a_m g_2 \\
a_{14} &= -b_n g_1/g_3, \qquad a_{16} = -r_\eta/g_3 \\
a_{24} &= a_m g_2/g_4, \qquad a_{27} = -1/g_4 \\
a_{31} &= b_n\big(c^2 g_6 + s^2 g_7\big)/g_5 \\
a_{32} &= -a_m r_\eta\big(c^2 g_7 + s^2 g_6\big)/g_5, \qquad a_{33} = a_{31}/b_n \\
a_{35} &= r_\eta(\hat{r}_z e_{33} - \lambda_z\kappa_z)/g_5, \qquad a_{38} = -r_\eta\kappa_z/g_5 \\
a_{39} &= -r_\eta e_{zz}/g_5, \qquad a_{41} = -b_n(c^2 g_8 + s^2 g_9)/g_5 \\
a_{42} &= -a_m r_\eta\big(c^2 g_9 + s^2 g_8\big)/g_5, \qquad a_{43} = a_{41}/b_n \\
a_{45} &= -r_\eta(\hat{r}_z c_{zz} - \lambda_z e_{zz})/g_5, \qquad a_{48} = -r_\eta e_{zz}/g_5 \\
a_{49} &= r_\eta c_{zz}/g_5, \qquad a_{61} = b_n^2\big(c^4 g_{10} + s^4 g_{11}\big) - a_m^2 G_{x\theta} r_\eta^2 \\
a_{62} &= -a_m b_n r_\eta(g_{12}/g_5 - c_{x\theta} - G_{x\theta}) \\
a_{63} &= -\big(a_{61} + a_m G_{x\theta} r_\eta^2\big)/b_n \\
a_{65} &= -b_n\big[c^2(\hat{r}_z g_9 + \lambda_z g_7 - \lambda_x g_5) + s^2(\hat{r}_z g_8 + \lambda_z g_6 - \lambda_\theta g_5)\big]/g_5 \\
a_{68} &= -b_n\big(c^2 g_6 + s^2 g_7\big) r_\eta/g_5 \\
a_{69} &= -b_n\big(-c^2 g_8 - s^2 g_9\big) r_\eta/g_5 \\
a_{72} &= a_m^2\big(c^4 g_{11} + s^4 g_{10}\big) r_\eta^2 g_5 - b_n^2 G_{x\theta} \\
a_{73} &= -a_m r_\eta(g_{12}/g_5 + c_{x\theta}) \\
a_{75} &= a_m r_\eta^2\big[c^2(\hat{r}_z g_8 + \lambda_z g_6 - \lambda_\theta g_5) + s^2(\hat{r}_z g_9 + \lambda_z g_7 - \lambda_x g_5)\big]/g_5 \\
a_{78} &= a_m\big(c^2 g_7 + s^2 g_6\big) r_\eta^2/g_5 \\
a_{79} &= a_m\big(-c^2 g_9 - s^2 g_8\big) r_\eta/g_5 \\
a_{83} &= \big(c^4 g_{10} + s^4 g_{11}\big)/g_5, \qquad a_{85} = a_{65}/b_n \\
a_{88} &= -r_\eta\big[\big(c^2 g_6 + s^2 g_7\big)/g_5 - 1\big] \\
a_{89} &= r_\eta\big(c^2 g_8 + s^2 g_9\big)/g_5, \qquad a_{91} = -b_n g_1 \\
a_{93} &= -b_n^2 g_1 - a_m^2 g_2 \\
a_{94} &= b_n^2\big(c^2\kappa_\theta + s^2\kappa_x\big) + r_\eta^2 a_m^2\big(c^2\kappa_x + s^2\kappa_\theta\big) \\
a_{10,5} &= b_n^2\big(c^2 k_\theta + s^2 k_x\big) + r_\eta^2 a_m^2\big(c^2 k_x + s^2 k_\theta\big) \\
g_1 &= c^2 e_{\theta\theta z} + s^2 e_{xxz}, \qquad g_2 = s^2 e_{\theta\theta z} + c^2 e_{xxz} \\
g_3 &= c^2 G_{\theta z} + s^2 G_{xz}, \qquad g_4 = c^2 G_{xz} + s^2 G_{\theta z} \\
g_5 &= e_{zz}^2 + c_{zz}\kappa_z, \qquad g_6 = e_{z\theta} e_{zz} + c_{\theta z}\kappa_z \\
g_7 &= e_{zx} e_{zz} + c_{xz}\kappa_z, \qquad g_8 = c_{zz} e_{z\theta} - c_{\theta z} e_{zz} \\
g_9 &= c_{zz} e_{zx} - c_{xz} e_{zz} \\
g_{10} &= -c_{zz} e_{z\theta}^2 + 2c_{\theta z} e_{z\theta} e_{zz} - c_{\theta\theta} e_{zz}^2 + c_{\theta z}^2\kappa_z - c_{\theta\theta} c_{zz}\kappa_z \\
g_{11} &= -c_{zz} e_{zx}^2 + 2c_{xz} e_{zx} e_{zz} - c_{xx} e_{zz}^2 + c_{xz}^2\kappa_z - c_{xx} c_{zz}\kappa_z \\
g_{12} &= -c_{zz} e_{z\theta} e_{z\theta} + c_{xz} e_{z\theta} e_{zz} + c_{\theta z} e_{z\theta} e_{zz} + c_{\theta z} c_{xz}\kappa_z
\end{aligned}$$

where $c = \cos\alpha$ and $s = \sin\alpha$, and α is the fiber orientation angle.

The elements of $\boldsymbol{M}^{(\eta)}$ in Eq. (24) are zero except for $\boldsymbol{M}^{(\eta)}(4, 1) = g_1$ and $\boldsymbol{M}^{(\eta)}(5, 2) = g_2$. The matrix $\boldsymbol{H}^{(\eta)}$ in Eq. (24) are

$$\boldsymbol{H}^{(\eta)} = \begin{bmatrix} h_{11} & h_{12} & h_{13} & 0 & h_{15} & 0 & 0 & h_{18} & h_{19} & 0 \\ h_{21} & h_{22} & h_{23} & 0 & h_{25} & 0 & 0 & h_{28} & h_{29} & 0 \\ h_{31} & h_{32} & 0 & 0 & 0 & 0 & 0 & 0 & 0 & 0 \\ h_{41} & 0 & h_{43} & h_{44} & 0 & 0 & 0 & 0 & 0 & 0 \\ 0 & 0 & h_{53} & h_{54} & 0 & 0 & 0 & 0 & 0 & 0 \\ 0 & 0 & 0 & 0 & h_{65} & 0 & 0 & 0 & 0 & 0 \\ 0 & 0 & 0 & 0 & h_{75} & 0 & 0 & 0 & 0 & 0 \end{bmatrix}$$

$$h_{11} = -b_n\left(c^4 g_{10} + s^4 g_{11}\right)/[g_5(r_\eta + z)]$$

$$h_{12} = a_m(g_{12}/g_5 - c_{\theta z}), \qquad h_{13} = -h_{11}/b_n$$

$$h_{15} = -a_{85}/r_\eta, \qquad h_{18} = \left(c^2 g_6 + s^2 g_7\right)/g_5$$

$$h_{19} = -\left(c^2 g_8 + s^2 g_9\right)/g_5, \qquad h_{21} = -b_n(g_{12}/g_5 - c_{\theta x})/(r_\eta + z)$$

$$h_{22} = a_m\left(c^4 g_{11} + s^4 g_{10}\right)/g_5, \qquad h_{23} = h_{21}/b_n$$

$$h_{25} = -a_{65}/b_n, \qquad h_{28} = \left(c^2 g_7 + s^2 g_6\right)/g_5$$

$$h_{29} = -\left(c^2 g_9 + s^2 g_8\right)/g_5, \qquad h_{31} = a_m G_{x\theta}$$

$$h_{32} = -b_n G_{x\theta}/(r_\eta + z), \qquad h_{41} = -g_1/(r_\eta + z)$$

$$h_{43} = b_n h_{41}, \qquad h_{44} = b_n\left(c^2\kappa_\theta + s^2\kappa_x\right)/(r_\eta + z)$$

$$h_{53} = a_m g_2, \qquad h_{54} = -a_m\left(c^2\kappa_x + s^2\kappa_\theta\right)$$

$$h_{65} = b_n\left(c^2 k_\theta + s^2 k_x\right)/(r_\eta + z), \qquad h_{75} = -a_m\left(c^2 k_x + s^2 k_\theta\right)$$

The relations of the material parameters between $\{e_{zx}, e_{z\theta}, e_{zz}, e_{\theta\theta z}, e_{xxz}\}$, $\{\lambda_x, \lambda_\theta, \lambda_z\}$, and $\{c_{xx}, c_{x\theta}, c_{xr}, c_{\theta\theta}, c_{\theta r}, c_{rr}, G_{\theta r}, G_{xr}, G_{x\theta}\}$ in the above matrices and $\{d_{zx}, d_{z\theta}, d_{zz}, d_{\theta\theta z}, d_{xxz}\}$, $\{\alpha_x, \alpha_\theta, \alpha_z\}$ or $\{\alpha_L, \alpha_T\}$, and $\{E_x, E_\theta, E_z, G_{\theta z}, G_{xz}, G_{x\theta}, \upsilon_{\theta z}, \upsilon_{xz}, \upsilon_{x\theta}\}$ or $\{E_L, E_T, G_{LT}, G_{TT}, \upsilon_{LT}, \upsilon_{TT}\}$ in Table 1, respectively, can be found in Refs. 20 and 21.

References

[1]Bailey, T., and Hubbard, J. E., "Distributed Piezoelectric–Polymer Active Vibration Control of a Cantilever Beam," *Journal of Guidance, Control, and Dynamics*, Vol. 8, No. 5, 1985, pp. 605–611.

[2]Crawley, E., and de Luis, J., "Use of Piezoelectric Actuators as Element of Intelligent Structures," *AIAA Journal*, Vol. 25, No. 10, 1987, pp. 1373–1385.

[3]Lee, C. K., and Moon, F. C., "Laminated Piezopolymer Plates for Torsion and Bending Sensors and Actuators," *Journal of the Acoustical Society of America*, Vol. 85, No. 6, 1989, pp. 2432–2439.

[4]Srinivas, S., "Analysis of Laminated, Composite, Circular Cylindrical Shells with General Boundary Conditions," NASA TR-R-412, 1974.

[5]Ren, J. G., "Analysis of Simply-Supported Laminated Circular Cylindrical Shell Roofs," *Composite Structures*, Vol. 11, No. 2, 1989, pp. 277–292.

[6]Fan, J., and Zhang, J., "Analytical Solutions for Thick, Doubly Curved, Laminated Shells," *Journal of Engineering Mechanics*, Vol. 118, No. 7, 1992, pp. 1338–1356.

[7]Huang, N. N., and Tauchert, T. R., "Thermoelastic Solution for Cross-Ply Cylindrical Panels," *Journal of Thermal Stresses*, Vol. 14, No. 2, 1991, pp. 227–237.

[8]Huang, N. N., and Tauchert, T. R., "Thermoelastic Stresses in Doubly-Curved Cross-Ply Laminates," *International Journal of Solids and Structures*, Vol. 28, No. 8, 1992, pp. 991–1000.

[9]Noor, A. K., Peters, J. M., and Burton, W. S., "Three-Dimensional Solutions for Initially Stressed Structural Sandwiches," *Journal of Engineering Mechanics*, Vol. 120, No. 2, 1994, pp. 284–303.

[10]Burton, W. S., and Noor, A. K., "Three-Dimensional Solutions for Thermomechanical Stresses in Sandwich Panels and Shells," *Journal of Engineering Mechanics*, Vol. 120, No. 10, 1994, pp. 2044–2071.

[11]Tzou, H. S., "A New Distributed Sensor and Actuator Theory for 'Intelligent' Shell," *Journal of Sound and Vibration*, Vol. 153, No. 2, 1992, pp. 335–349.

[12]Zhou, S., Liang, C., and Rogers, C. A., "Impedance Modeling of Two-Dimensional Piezoelectric Actuators Bounded on a Cylinder," *Proceedings of ASME Adaptive Structures and Material Systems*, AD-Vol. 35, 1993, pp. 247–255.

[13]Chandrashekhara, K., and Kolli, M., "Thermally Induced Vibration of Adaptive Doubly Curved Composite Shells with Piezoelectric Devices," *Proceedings of the AIAA/ASME/ASCE/AHS/ASC 36th Structures, Structural Dynamics, and Materials Conference*, AIAA, Washington, DC, 1995, pp. 1628–1636 (AIAA Paper 95-1352).

[14]Yang, J. S., Batra, R. C., and Liang, X. Q., "The Vibration of a Simply Supported Rectangular Elastic Plate Due to Piezoelectric Actuators," *International Journal of Solids and Structures* (to be published).

[15]Xu, K., Noor, A. K., and Tang, Y. Y., "Three-Dimensional Solutions for Free Vibrations of Initially-Stressed Thermoelectroelastic Multilayered Plates," *Computer Methods in Applied Mechanics and Engineering* (to be published).

[16]Seely, S., and Poularikas, A., *Electromagnetics, Classical and Modern Theory and Applications*, Marcel Dekker, New York, 1979.

[17]Washizu, K., *Variational Methods in Elasticity and Plasticity*, Pergamon, Elmsford, NY, 1982.

[18]Xu, K., Noor, A. K., and Tang, Y. Y., "Three-Dimensional Solutions for Coupled Thermoelectroelastic Response of Multilayered Plates," *Computer Methods in Applied Mechanics and Engineering*, Vol. 126, No. 2, 1995, pp. 355–371.

[19]Nelson, R., "Simplified Calculation of Eigenvector Derivatives," *AIAA Journal*, Vol. 14, No. 9, 1976, pp. 1201–1205.

[20]Jones, R. M., *Mechanics of Composite Materials*, Scripta, Washington, DC, 1975.

[21]Nowacki, W., *Dynamic Problems of Thermoelasticity*, Noordhoff International, Leyden, The Netherlands, 1975.